In Vivo Regenerative Properties of Coralline-Derived (Biocoral) Scaffold Grafts in Human Maxillary Defects: Demonstrative and Comparative Study with Beta-Tricalcium Phosphate and Biphasic Calcium Phosphate by Synchrotron Radiation X-Ray Microtomography

Alessandra Giuliani, PhD;[*] Adrian Manescu, PhD;[†] Emanuel Larsson, PhD;[‡,§] Giuliana Tromba, PhD;[§] Giuseppe Luongo, MD, DDS;[¶] Adriano Piattelli, MD, DDS;[**] Francesco Mangano, DDS;[††] Giovanna Iezzi, DDS, PhD;[‡‡] Carlo Mangano, MD, DDS[§§]

ABSTRACT

Background: In recent years, there has been interest on the fabrication of systems using particulates or block-based approach for bone tissue engineering (TE) scaffolds, possessing porous interconnected structures. In fact, these particular morphologies greatly increase the surface area for more chemical and biological reactions to take place.

Purpose: This study was designed to demonstrate the unique capability of the synchrotron radiation x-ray microtomography (micro-CT) in offering an advanced characterization of coralline-derived (Biocoral) biomaterials placed in human maxillary defects as it allows, in a nondestructive way, a complete, precise, and high-resolution three-dimensional analysis of their microstructural parameters. Moreover, the comparison between Biocoral and other biomaterials was explored to understand the mechanism of their biological behavior as bone substitute.

Materials and Methods: Implant survival, bone regeneration, graft resorption, neovascularization, and morphometric parameters (including anisotropy and connectivity index of the structures) were evaluated by micro-CT in Biocoral and the other biomaterials after 6 to 7 months from implantation in human maxillary bone defects.

Results: After the in vivo tests, a huge amount of bone was detected in the retrieved Biocoral-based samples, coupled with a good rate of biomaterial resorption and the formation of a homogeneous and rich net of new vessels. The morphometric parameters were comparable to those obtained in the biphasic calcium phosphate-based control, with the exception of the connectivity index for which this control exhibited the most well-connected structure. This last result, together with those referred to the poor performances of the β-tricalcium phosphate block-based sample, suggests that the particular scaffold morphology may play a role in the hunt the optimal scaffold structure to be implanted.

Conclusion: In this limited study, implant success rate seems not strictly dependent on the biomaterial that is used, but on the scaffold morphology. Micro-CT technique was demonstrated to play a fundamental role in advanced characterization of bone TE constructs.

KEY WORDS: biomaterials, bone regeneration, micro-CT

[*]Dip. di Scienze Cliniche Specialistiche e Odontostomatologiche – Sezione di Biochimica, Biologia e Fisica Applicata, Università Politecnica delle Marche, Ancona, Italy; [†]Dip. di Scienze Cliniche Specialistiche e Odontostomatologiche – Sezione di Biochimica, Biologia e Fisica Applicata, Università Politecnica delle Marche, Ancona, Italy; [‡]Department of Engineering and Architecture, Università di Trieste, Trieste, Italy; [§]Sincrotrone Trieste S.C.p.A, Basovizza (Trieste), Italy; [¶]Department of Maxillo Facial Surgery, Federico II University, Naples, Italy; [**]Department of Medical, Oral and Biotechnological Sciences, University of Chieti-Pescara, Chieti, Italy; [††]private practice, Gravedona (Como), Italy; [‡‡]Department of Medical, Oral and Biotechnological Sciences, University of Chieti-Pescara, Chieti, Italy; [§§]Department of Surgical and Morphological Sciences, University of Insubria, Varese, Italy

Reprint requests: Dr. Alessandra Giuliani, Dip. di Scienze Cliniche Specialistiche e Odontostomatologiche, Università Politecnica delle Marche, Via Brecce Bianche 1, Ancona 60131, Italy; e-mail: a.giuliani@univpm.it

DOI 10.1111/cid.12039

INTRODUCTION

Tissue engineering (TE) has emerged as a promising approach for the repair and regeneration of tissues and organs that are lost, damaged, or in general functionally compromised as a result of trauma, injury, disease, or aging.[1,2]

A key component of TE approach to bone regeneration is represented by natural or man-made scaffold that acts as a template for cell interactions and formation of bone extracellular matrix providing structural support to the newly formed tissue.[3] An ideal scaffold should fulfill a complex set of characteristics; in summary, it should (i) be three dimensional and highly porous with an interconnected pore network for allowing cell migration and growth, as well as flow transport of nutrients and metabolic waste; (ii) be biocompatible and preferably bioresorbable with a controllable resorption rate matching that of bone repair; (iii) exhibit a surface chemistry suitable for cell attachment, proliferation, and differentiation; (iv) have mechanical properties comparable to those of the tissues at the site of implantation; and (v) have the potential to be commercially produced and safely sterilized without any alteration of its properties.[3–7]

Regarding materials for use in bone TE, several approaches have been shown to be effective in stimulating bone regeneration, and ceramics especially excel in this regard.[8,9] Notwithstanding the stimulatory effect of bioactive ceramics on bone tissue formation, there is a continuous need to explore avenues in which materials, cells, and biologically active molecules are combined. This is critical because cells and growth factors are the two key elements when discussing bone biology/healing, their interaction being fundamental for an effective regeneration process. Although continuous progress is being made in understanding osseous healing process, these new insights have not readily found their way into effective TE approaches. The combination of materials, cells, and growth factors seems to be the recipe for a truly effective bone TE strategy. A system designed for bone repair would ideally combine osteoconductive and osteoinductive properties, in a way that new bone formation can be enhanced through an adequately shaped three-dimensional scaffold (osteoconduction) and by a biological stimulus (osteoinduction).[10] Ceramic materials, due to their inorganic nature and ionic composition, are adequate for bone applications. Examples of ceramic materials are calcium phosphates, such as hydroxyapatite (HA), tricalcium phosphate (TCP), and coralline-derived calcium phosphate, known for their ability to bond to and stimulate bone regeneration.[9,11–13] In recent years, there has been interest on the fabrication of three-dimensional systems using particulates or block-based approach for a TE scaffold, possessing a porous interconnected structure. This is an extremely interesting strategy, as it provides a potential to overcome normally encountered problems associated with porosity of the scaffold. Additionally, with particle or block-based systems shaped as scaffolds, the surface area for more chemical and biological reactions to take place is greatly increased.[14]

The formation of three-dimensional scaffolds from biomaterials in particulate or block form creates the potential for these systems to be used either in an acellular strategy (implanting of the scaffold and colonization of it by surrounding cells) or combining it with cells in vitro, creating a hybrid cell–material construct. Simultaneously, these scaffolds can also be used as delivery systems, having a multifunctional purpose – support and release of bioactive agents – enhancing the regenerative potential of the system.

The clinical use in bone regeneration of coralline-derived biomaterial (Biocoral) needs to know the biomechanical and biological parameters of this biomaterial and its behavior when implanted in bone. Moreover, the comparison between Biocoral and other biomaterial is interesting, as β-TCP, to understand the mechanism of their biological behavior as bone substitute.

X-ray computed microtomography (micro-CT) is a powerful tool for scaffold characterization. Unlike many other techniques for pore shape, size, and distribution assessment, such as scanning electron microscopy (SEM) and mercury intrusion porosimetry, micro-CT can nondestructively obtain a three-dimensional image of a scaffold.[15] When combined with three-dimensional image analysis techniques, micro-CT can therefore provide not only qualitative but also quantitative information on the scaffold structure.[16,17]

The ability of micro-CT to image three-dimensional structures in a nondestructive way has made its use and application extremely popular across several disciplines including physics, materials science, medicine, mineral processing, and powder technology. In addition, the availability of synchrotron radiation x-ray sources has further stimulated the application of micro-CT due to its numerous advantages with respect

to conventional x-ray sources, including higher beam intensity, higher spatial coherence, and monochromaticity. This work exploits mainly the monochromaticity property of synchrotron radiation because it reduces significantly the beam hardening effects, thus allowing to simplify the segmentation process of the whole image analysis.

In the present study, synchrotron radiation x-ray micro-CT was used to analyze the three-dimensional porous architecture and microstructure of coralline-derived calcium phosphate scaffolds after long-term in vivo tests on humans; the results obtained on Biocoral were compared with those referred to other biomaterial, as β-TCP or TCP in combination with HA, to understand the mechanism of their biological behavior as bone substitute. Although micro-CT studies on bioactive TCP or TCP in combination with HA were reported in the last years literature,[18–22] to the best of the authors' knowledge, investigation on Biocoral scaffolds has been documented up to now.[23] In this research work, micro-CT was demonstrated to possess the unique capability of analyzing in detail the Biocoral scaffold three-dimensional structure in terms of pore size, strut thickness (STh), and degree of pore interconnection, as well as the three-dimensional distribution of the newly formed bone on scaffold walls. Furthermore, a comparison between architectural features and bioactive behavior of Biocoral and β-TCP or TCP in combination with HA was presented and discussed in order to confirm and extend the promising results of previous studies about the suitability of Biocoral as effective biomaterial for scaffolding.[24,25]

MATERIALS AND METHODS

Twelve healthy patients with noncontributory medical history (five women and seven men, all nonsmokers, mean age of 62 years, range 55–71 years) were included in this study. The protocol of the study was approved by the Ethical Committee of the University of Chieti, Italy. All patients signed a written informed consent form. All patients were candidates for augmentation in the posterior area of maxilla to receive fixed restorations and were divided in three groups of four patients for every biomaterial. The inclusion criteria were the following: partially edentulous patients with a bilateral loss of teeth in the maxillary premolar or molar areas with an alveolar atrophy that needs preimplant bone regeneration. The exclusion criteria were the following: severe illness, head and neck radiation therapy, chemotherapy, uncontrolled diabetes, uncontrolled periodontal disease, and smoking. After a thorough oral and physical examination, patients were scheduled for bone reconstruction procedures. At surgery day, the patients' mouths were rinsed with a chlorhexidine digluconate solution 0.12% for 2 minutes prior to surgery. Local anesthesia using Articaine® (Ubistesin 4% – Espe Dental AG, Seefeld, Germany) and epinephrine 1:100 was performed. A crestal incision was made, with buccal releasing incisions medially and distally. Full thickness flaps were then elevated, exposing the alveolar crest. The horizontal and vertical defects were filled with blocks and granular biomaterial according to the three selected materials, namely, the Biocoral, β-TCP, and 70% β-TCP/30% HA. After 6 or 7 months from bone augmentation, at the implant sites before drill preparation, samples of regenerated bone were harvested by trephine bur.

Scaffolds Preparation

"Biocoral®" (Leader Italia, Milan, Italy) is mainly composed of calcium carbonate in the form of aragonite (97–98%), strontium, fluoride, magnesium, sodium, and potassium.[26–29] It has a porosity of more than 45%, with pores of about 250 μm (range 150–400) in diameter, resembling spongious bone. Several components are present at levels equivalent to those found in mammalian bone, notably trace elements, which play a vital role in the process of mineralization and in the activation of enzymatic reactions in bone cells. Two trace elements have specific effects: strontium is involved in the formation and growth of the crystalline component of bone, protects calcification mechanisms, and increases mineralization. Furthermore, strontium levels are higher in the most active bone structure, i.e., the metaphysis and bone callus. Fluorine – in proper quantity – increases bone formation by direct effects on proliferation of cellular precursors of osteoblasts. Biocoral® pore size is important as this offers the ideal environment for vascularization and migration of osteoclasts and osteoblasts. It ranges between 20 and 50%, depending on the species selected. Natural calcium carbonates with different porosities can be used according to the operating procedure. Biocoral® pore size ranges between 150 and 500 μm, depending on the species, selected according to clinical indications. It has previously been shown that these sizes are optimal for occupation by fluids and bone marrow cells in order to complete mineralized

newly formed bone. Bone cells (bone marrow and blood of the recipient bone) can freely invade the open porous structure of Biocoral® deep in its core. This cellular invasion determines the first phase of the bone restoration process characterized by the development of a neovascularization. Some corals (Porites in particular) have the architecture similar with the cancellous bone. Recently, it has been found that Biocoral may be used as a bone replacement material for the treatment of osseous defects associated with adult periodontitis.[30] In the open pores, there is a formation of a fibrovascular tissue that is progressively replaced by bone.

"β-TCP" (Kasios, Leader Italia) is a synthetic bone substitute with partial interconnection. The β-TCP blocks were produced by using the foam technology as previously reported.[31] Briefly, a slurry containing 25 g of β-TCP was prepared with distilled water and used to substantially impregnate a block of polyurethane foam under vacuum. This ensured that the ceramic coated the polyurethane walls to produce a replica of the reticulated foam material, the ceramic parts of the biomaterial being centered by the polymer. The blocks of polyurethane impregnated with the slurry were then dried in an oven and heated in a furnace oven at 800°C; this led to a complete burn of the organic polyurethane foam. The three-dimensional scaffolds of β -TCP were then sintered at a temperature >1200°C.

The "HA/TCP" (Leader Italia) ceramic scaffolds used in this study were fabricated by the direct rapid prototyping technique dispense plotting.[32] A virtual scaffold model was designed with a cylindrical outer geometry by using three-dimensional computer-aided design software (Solid Works, Waltham, MA, USA). The size of the model was adapted to the shrinkage of the ceramic material in the subsequent sintering process. The inner geometry, i.e., the pathway of the material rods, was defined by custom-made software that generates the control commands of the rapid prototyping machine. To build up the green bodies, material rods, consisting of a paste-like aqueous ceramic slurry, were extruded out of a cartridge through a nozzle and deposited using an industrial robot (GLT mbH, Pforzheim, Germany). In this study, HA and TCP powders (Merck, Darmstadt, Germany) were blended to get a powder mixture with a HA/TCP weight ratio of 30/70. The characteristic rheological behavior of the aqueous ceramic slurry was achieved by thermal treatment of the raw HA powder at 900°C for 1 hour and by adding a compatible binder/dispersant system of organic additives of 10.5 wt% relative to the mass of ceramic powder. The rod deposition was controlled in *x*, *y*, and *z* directions to assemble three-dimensional scaffolds layer by layer on a building platform. By rotating the direction of the rod deposition by 60° from layer to layer, a three-dimensional network with an interconnecting pore structure was generated. The assemblies made of ceramic slurry were dried at room temperature and subsequently sintered at 1250°C for 1 hour. Finally, the sintered scaffolds were manually reduced to smaller blocks with a volume of about 1.4 cm^3 in order to remove the solid rim that resulted from the turning points at the edge of the printed pathways.

Scaffold Characterization

Biocoral, β-TCP, and 70% TCP/30% HA scaffolds were processed following the protocols in use at the Human Morphology Laboratory of the Insubria University in Varese.

Being dry and inorganic, these specimens did not require fixation or dehydration and were simply fractured in order to obtain an uncontaminated surface. The fragments were glued onto standard aluminum stubs with conductive adhesives and gold coated in an argon atmosphere by means of an Emitech K-550 sputter coater in order to make them conductive. All specimens were then observed with a FEI XL-30 FEG high-resolution field-effect SEM operated at an accelerating voltage of 7 to 10 kV and fitted with an Everhart-Thornley detector for secondary electron imaging. All specimens were observed at different magnifications and different angles, and electron micrographs were directly obtained in digital form as 1424 × 968 pixel, 8-bpp grayscale TIFF files. The micrographic images of the three selected scaffolds, namely, the Biocoral, the β-TCP, and the 70% TCP/30% HA, are shown in Figure 1.

Microstructural Analysis by X-Ray Micro-CT

While histological investigation was performed in the complete set of retrieved samples, due to the demonstrative nature of the present work, the micro-CT measurements were carried out on four different samples, namely, a Biocoral scaffold as such, a Biocoral scaffold after in vivo test for 6 months, Biocoral beads in combination with a β-TCP block after in vivo test for 6 months, and a 70% TCP/30% HA scaffold after permanence in vivo for 7 months. The sample referred to

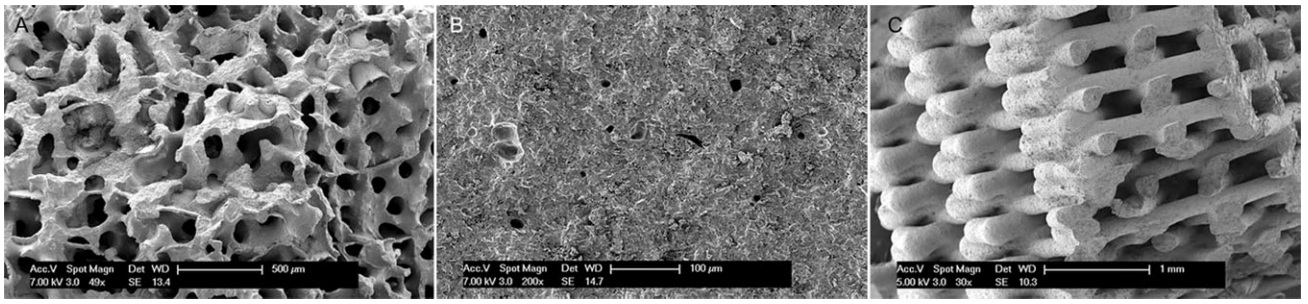

Figure 1 Secondary electron images of the scaffolds before the in vivo tests. (A) Biocoral shows large, irregular, and interconnected cavities in the 100- to 200-µm range, separated by solid walls 10 to 50 µm thick. (B) β-tricalcium phosphate (TCP) blocks show a smoother and more compact mass, with a vitreous fracture and a large number of small, heterogeneous, and partially interconnected pores. (C) The biphasic hydroxyapatite (70% TCP/30% hydroxyapatite) shows a three-dimensional grid-like structure, highly reminiscent of cancellous bone. Slender rods, 200 µm thick, were stratified and partially fused in order to define intercommunicating spaces in the 100- to 250-µm range.

Biocoral beads in combination with a β-TCP block arrived fractured and two parts of it were investigated separately.

Experimental Setup. Micro-CT experiments were performed at the SYRMEP beamline of the ELETTRA Synchrotron Radiation Facility (Trieste, Italy). The experimental conditions were selected, according to the properties of the samples. Due to the sample composition, the energy of the monochromatic beam was set to 23 keV with a sample-to-detector distance of 70 mm, the voxel size was $9 \times 9 \times 9$ µm.[3] The reconstruction of the tomographic slices was carried out using a custom-developed software,[33] applying the standard filtered back-projection algorithm.[34] The exposure time was set to around 3 seconds per projection, with a total of nine hundred radiographic images for each sample.

Image Segmentation. A three-dimensional median smoothing filter (kernel width = 3) was applied in order to facilitate further segmentation. Three peaks can clearly be distinguished (background, newly formed bone – in the samples investigated after implantation, and scaffold material). After examining the histograms, representative threshold values were manually set to 75 (newly formed bone) and one hundred fourteen (scaffold). Figure 2 reports the histogram for each considered scaffold as obtained excluding the histogram portion with the gray levels < 70, i.e., the portion referred to background and soft tissues.

Extraction of Quantitative Parameters. The volume data were analyzed by using the VG Studio MAX 1.2 software (Volume Graphics GmbH, Heidelberg, Germany) and the Pore3D[35] software library (SYRMEP research group of the Elettra Synchrotron Light Laboratory, Trieste, Italy). Quantitative parameters were calculated directly from three-dimensional images to characterize the different implants. In the Biocoral sample investigated before implantation, such segmentation was easily performed by simple thresholding because the gray level histogram was clearly bimodal with a first peak corresponding to air and a second peak corresponding to scaffold (Figure 2A). However, after in vivo tests, an intermediate peak related to a newly formed bone appeared (Figure 2, A–C) in all the investigated samples. The sample that arrived fractured, referred to Biocoral beads in combination with a β-TCP block, was investigated considering two different volumes (fragments) separately. The histograms of the two separated subvolumes and that referring to their sum are reported in Figure 2B. Furthermore, in the 70% TCP/30% HA scaffold investigated after 7 months of implantation, it is possible to segment two different peaks strictly referred to the two scaffold phases (Figure 2C). The quantification of the different phases (including a rough estimation of the vessel amount) present inside the different samples is reported in Table 1 for the full-retrieved specimens.

Thin three-dimensional sections are represented in Figure 3 in order to better visualize the newly formed bone-scaffold interface, together with the evidence of the presence of a newly formed vascularization net. In fact, while conventional micro-CT setups lack the sensitivity to resolve the fibrous tissue and the vascularization, the chosen synchrotron radiation micro-CT setup (containing not only absorption but also phase-contrast signals) allows also the visualization of these unmineralized tissues.

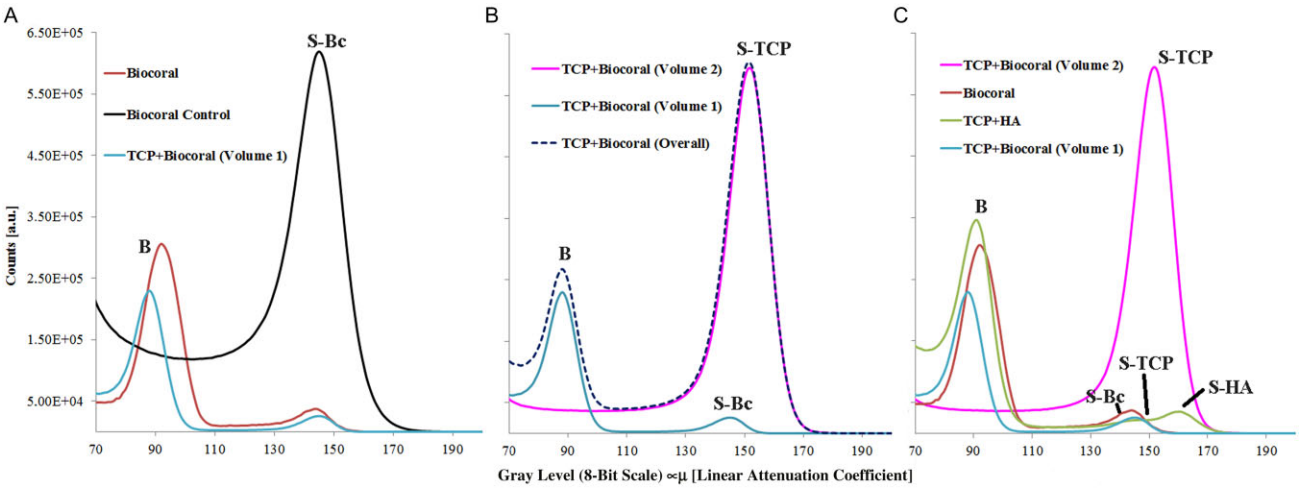

Figure 2 (A) Gray level histogram of the coralline-derived biomaterial (Biocoral) scaffold as retrieved from in vivo test after 6 months. Data are compared with the same coralline-derived biomaterial (Biocoral control) as it is after production and with the histogram referred to the sample made of Biocoral beads in combination with β-TCP blocks (volume I) as retrieved from in vivo test after 6 months (TCP + Biocoral). (B) Gray level histogram of the two fragments of the sample made of Biocoral beads in combination with β-TCP blocks as retrieved from in vivo test after 6 months and the sum of their histograms (overall). (C) Comparison of the gray level histogram of the coralline-derived biomaterial (Biocoral) scaffold (as retrieved from in vivo test after 6 months) with the sample made of Biocoral beads in combination with β-TCP blocks (as well retrieved from in vivo test after 6 months) and the three-dimensional scaffold composed by HA and β-TCP in a ratio of 30/70 (as retrieved from human site after a period of 7 months). The first peak on the left, corresponding to the background absorption of air, was not reported in all the histograms (the gray level scale start from the value of 70). Legend: B = bone; S-Bc = biocoral scaffold; S-TCP = tricalcium phosphate scaffold; S-HA = hydroxyapatite scaffold.

Representative $1.35 \times 1.35 \times 1.35$ mm^3 subvolumes (the largest cubic three-dimensional portion fully included in the smallest sample bulk) were then analyzed based on the structural indices usually measured for bone samples.[36] Two different structural analyses were performed: the first one (Table 2) referred to the whole mineralized tissue (including the scaffold and the newly formed bone) and the second one specifically referred to the newly formed bone (Table 3). The following morphometric parameters were evaluated for the whole mineralized tissue (Table 2): total volume (TV – expressed in cubic micrometer) of the volume of interest; sample volume (SV – expressed in cubic micrometer); SV to TV ratio (SV/TV – expressed as a percentage); sample surface to SV ratio (SS/SV – per millimeter); STh (expressed in micrometers); strut number (SNr – per millimeter); and strut separation (expressed in micrometers).

For the evaluation of the regenerated bone structural analysis (Table 3), the same quantitative descriptors applied to the whole mineralized tissue were used in order to detect bone volume (BV – expressed in cubic

TABLE 1 Three-Dimensional Quantitative Analysis of the Different Phases after In Vivo Tests. The Whole Retrieved Samples Are Considered

Phases	Pure Biocoral	Biocoral + TCP (*volume I*)	Biocoral + TCP (*volume II*)	70% TCP/ 30% HA
Vessels (μm^3) (*rough estimation*)	1.7×10^9	0.9×10^9	1.5×10^9	2.0×10^9
Newly formed bone (μm^3)	6.1×10^9	2.4×10^9	1.2×10^9	4.4×10^9
Scaffold (μm^3)				
Biocoral	0.2×10^9	0.3×10^9		
TCP			8.3×10^9	0.5×10^9
HA				0.3×10^9

HA = hydroxyapatite; TCP = tricalcium phosphate.

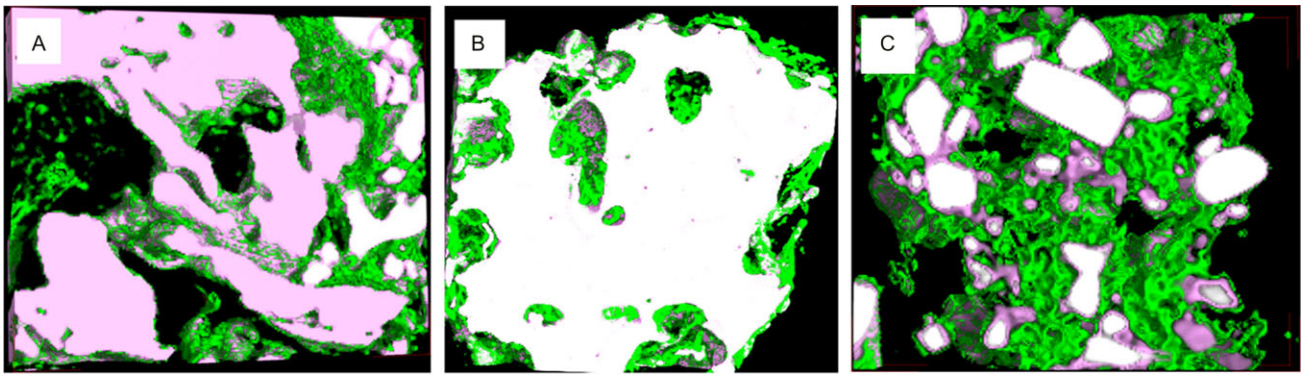

Figure 3 Representative $2.0 \times 1.6 \times 0.3$ mm^3 subvolumes (A) of the coralline-derived biomaterial (Biocoral) scaffold as retrieved from in vivo test after 6 months and (B) of the sample made of Biocoral beads in combination with a β-TCP block as retrieved from in vivo test after 6 months (TCP + Biocoral). Detail of the fragment (volume II) strictly referred to a β-TCP block. (C) Three-dimensional subvolume of the 70% β-TCP/30% HA sample as retrieved from in vivo test after 7 months. Legend: green phase = regenerated vessels; pink phase = newly formed bone; white phase = scaffold.

micrometer), BV to TV ratio (BV/TV – expressed as a percentage), bone surface to BV ratio (BS/BV – per millimeter), regenerated bone thickness (expressed in micrometers), etc.

Information about the anisotropy, i.e., the presence of preferential orientation(s) of the structure, was also extracted; this analysis was performed on the complete mineralized tissue (Table 4), but it was also restricted,

TABLE 2 Three-Dimensional Morphometric Analysis of the Constructs Retrieved from In Vivo Tests. Mineralized Tissues Are Considered (Scaffold + Newly Formed Bone)

	Pure Biocoral	Biocoral + TCP (*volume I*)	Biocoral + TCP (*volume II*)	70% TCP/30% HA
TV (μm^3)	2.46×10^9	2.46×10^9	2.46×10^9	2.46×10^9
SV (μm^3)	7.97×10^8	7.53×10^8	18.07×10^8	7.10×10^8
SS/SV (mm^{-1})	29	24	7	36
SV/TV (%)	32.4	30.6	73.5	28.9
Mean STh (μm)	69	84	294	55
Mean SNr (mm^{-1})	4.69	3.65	2.50	5.21
Mean SSp (mm)	144	190	106	137

HA = hydroxyapatite; SNr = strut number; SS = sample surface; SSp = strut separation; STh = strut thickness; SV = sample volume; TCP = tricalcium phosphate; TV = total volume.

TABLE 3 Three-Dimensional Morphometric Analysis of the Constructs Retrieved from In Vivo Tests. Only Newly Regenerated Bone Is Considered

	Pure Biocoral	Biocoral + TCP (*volume I*)	Biocoral + TCP (*volume II*)	70% TCP/30% HA
TV (μm^3)	2.46×10^9	2.46×10^9	2.46×10^9	2.46×10^9
BV (μm^3)	7.51×10^8	7.14×10^8	1.12×10^8	6.40×10^8
BS/BV (mm^{-1})	33	26	177	43
BV/TV (%)	30.5	29.0	4.6	26.0
Mean BTh (μm)	61	76	11	46
Mean BNr (mm^{-1})	5.00	3.82	4.03	5.65
Mean BSp (mm)	139	186	237	131

BNr = bone number; BS = bone surface; BSp = bone separation; BTh = bone thickness; BV = bone volume; HA = hydroxyapatite; TCP = tricalcium phosphate; TV = total volume.

TABLE 4 Three-Dimensional Anisotropy Analysis of the Constructs Retrieved from In Vivo Tests. Mineralized Tissues Are Considered (Scaffold + Newly Formed Bone)

	Pure Biocoral	Biocoral + TCP (volume I)	Biocoral + TCP (volume II)	70% TCP/30% HA
Isotropy index, *I* (–)	0.81	0.84	0.87	0.75
Elongation index, *E* (–)	0.10	0.07	0.09	0.05

HA = hydroxyapatite; TCP = tricalcium phosphate.

for the same TVs, to the newly regenerated bone (Table 5).

Anisotropic measurements of the retrieved samples, i.e., the presence of preferential orientations, were performed using the mean intercept length (MIL) method. The basic principle of the MIL method is to count the number of intersections between a linear grid and the pore-material interface as a function of the grid orientation ω.[37] The MIL (an intercept is the line between two intersections) is calculated as the ratio between the total length *L* of the line grid and the number of intersections. MIL measurements in three dimensional may be fitted to an ellipsoid, which can be expressed as the quadratic form of a second rank tensor *M*.[38] A fabric tensor *H* is defined as the inverse square root of *M*.[39,40] As the eigenvectors (u_1, u_2, u_3) of the fabric tensor *H* give information about the direction of the axes of the ellipsoid and the eigenvalues (t_1, t_2, t_3) express the radii of the ellipsoid, the latter can be used to define the degree of anisotropy, which denotes the ratio between the maximal and minimal radii of the MIL. In this article, the eigenvalues are summarized using the isotropy index $I = t_3/t_1$ and the elongation index $E = 1 - t_2/t_1$.[41] The isotropy index *I* measures the similarity of a fabric to a uniform distribution and varies between 0 (all observation confined to a single plane or axis) and 1 (perfect isotropy). The elongation index measures the preferred orientation of a fabric in the $[u_1,u_2]$ plane and varies between 0 (no preferred orientation) and 1 (a perfect preferred orientation with only parallel observations).

Finally, skeleton analysis was also applied in order to derive a descriptor for the interconnectivity.

Provided that the scaffold is a connected structure with almost no closed void cavities, a simple indicator of the connectedness of the three-dimensional complex pore space is the Euler number χ_V. For an open network structure, the Euler number may be calculated from the number of nodes *n* and the number of branches *b* after skeletonization of the pore space as $\chi_V = n - b$.[37] It provides a measure of connectivity, indicating the number of redundant connections: the breaking of a single connection will leave the network less connected increasing the value of χ_V, while the addition of a redundant connection will decrease it.[42] In order to normalize the Euler number with respect to the size of the considered volume *V*, the parameter "connectivity density" β computed as $\beta = (1 - \chi_V)/V$ is commonly adopted.[42] The connectivity density does not carry information about positions or size of connections, but it is a simple global measure of connectivity that gives higher values for better-connected structures and lower values for poorly connected structures.

RESULTS

Preliminary Electron Microscopy Analysis of the Scaffolds before In Vivo Tests

Biocoral specimens showed a very distinctive appearance: the whole mass of the specimen appeared made of large, irregular, and interconnected cavities in the

TABLE 5 Three-Dimensional Anisotropy Analysis of the Constructs Retrieved from In Vivo Tests. Only Newly Regenerated Bone Is Considered

	Pure Biocoral	Biocoral + TCP (volume I)	Biocoral + TCP (volume II)	70% TCP/30% HA
Isotropy index, *I* (–)	0.78	0.81	0.89	0.71
Elongation index, *E* (–)	0.11	0.09	0.05	0.08

HA = hydroxyapatite; TCP = tricalcium phosphate.

100- to 200-μm range, separated by solid walls 10 to 50 μm thick (Figure 1A). Neither smaller pores nor self-similar structures were visible. At higher magnification, the fracture surface reveals the walls as being made of needle-shaped crystalline particles tightly packed to form a solid, compact structure, where small pores or canalicular cavities are only occasionally visible. The natural surfaces are rather coarse and exhibit the ends of the needle-like crystals, whose fine, regular texture endows this material with a very high surface/volume ratio.

β-TCP blocks, by contrast, formed a smoother and more compact mass (Figure 1B) whose features became really appreciable only at a relatively high magnification. Under these conditions, the specimen showed a hard, compact appearance, with a vitreous fracture and a large number of small, heterogeneous, and partially interconnected pores, mostly in the micrometer range, irregularly dispersed across the specimen mass. The largest cavities showed the remains of rounded, and partially melted, particles, indicative of a sintering stage in the specimen processing.

The biphasic HA (70% TCP/30% HA) was made in form of a three-dimensional grid-like structure, highly reminiscent of cancellous bone (Figure 1C). Slender rods, 200 μm thick, were stratified and partially fused in order to define intercommunicating spaces in the 100- to 250-μm range. This structure is per se indicative of a good mechanical stability and of an unobstructed accessibility by the vascular network.

Micro-CT Analysis

Figure 2 reports the histogram for each considered sample as obtained excluding the histogram area with the gray levels < 70, i.e., the area referred to background and soft tissues. In Figure 2A, the gray level histogram of the coralline-derived biomaterial (Biocoral) scaffold (as retrieved from in vivo test after 6 months) was compared with the same coralline-derived biomaterial (Biocoral control) as it was before the in vivo test and with the histogram referred to the sample made of Biocoral beads in combination with β-TCP blocks (volume I) as retrieved from in vivo test after 6 months (TCP + Biocoral). Independently from the different volumetric dimensions of the retrieved samples, it was observed that after the in vivo tests, a huge amount of bone is detected in both the samples. This is demonstrated by the first peak on the left (gray value ~90), corresponding to the linear attenuation coefficient of the newly formed bone. Furthermore, it was noticed that all the right peaks in the histograms in Figure 1A correspond to a gray value ~144. This fact demonstrates that the fragment (volume I) of the sample made of Biocoral beads in combination with β-TCP blocks here considered presents residues of Biocoral beads without traces of β-TCP material. On the contrary, the second fragment (volume II) of the same sample (Figure 2B) presents a peak corresponding to a gray value ~155, corresponding to the linear attenuation coefficient of the β-TCP at the 23-keV experimental energy. This fact leaded the authors to consider the two fragments (volume I and volume II) of the sample made of Biocoral beads and β-TCP blocks separately, the former (volume I) describing the bioactivity of the Biocoral beads, the latter (volume II) the bioactivity of the β-TCP blocks. It has to be observed that, considering the histogram reported in Figure 2, B and C, the TCP blocks did not exhibit good performances in terms of bone regeneration (no peak was observed corresponding to bone): this finding is not new and was previously clinically and histologically observed by some of the authors (unpublished material). In Figure 2C it was also reported the comparison of the Biocoral bioactivity with the one referred to the three-dimensional scaffold composed by HA and β-TCP in the ratio of 30/70. It was found that after the in vivo tests, a huge amount of bone was detected in this last sample, as for those referred to Biocoral scaffolds.

Representative thin three-dimensional subvolumes are shown for each sample in Figure 3. In all the represented volumes, the vessel phase appears in green, the newly formed bone in pink, and the scaffold, independently from the specific biomaterial, in white. It was possible to detect newly formed vessels (even if at low resolution due to the experimental pixel size limit) because the chosen synchrotron radiation micro-CT setup, at the chosen experimental sample-to-detector distance, contains not only absorption but also phase-contrast signal, allowing also the visualization of these unmineralized tissues.

In the sample referred to the Biocoral scaffold (Figure 3A), a uniform distribution of vessels was detected together with a huge amount of bone, unlike the residual Biocoral, which was still not fully resorbed after the in vivo test of 6 months. These data were confirmed by the volumetric quantification of the different

phases (including a rough estimation of the vessel amount) performed in the different entire specimens and reported in Table 1. In the sample referred to the β-TCP block scaffold (Figure 3B), the results were completely different: a small amount of regenerated bone, almost surrounding and in adhesion with the peripheral TCP grains, was detected with few vessels located as well in the peripheral regions of the TCP block. Even these observations were confirmed by the quantitative volumetric analysis reported in Table 1 and referred to the whole TCP block (Biocoral + TCP volume II). Finally, in Figure 3C, a representative three-dimensional subvolume of the 70% β-TCP/30% HA sample, as retrieved from in vivo test after 7 months, is shown. In this sample, in analogy with the behavior of the Biocoral, an extended and uniform vascularization, together with a huge amount of newly regenerated bone, was observed. It can be assessed, based on Table 1 quantitative analysis (but also as shown on the histogram reported in Figure 2C) for this specific sample, that the bone regeneration is combined to the TCP resorption: in fact, the volumetric percentages change from 70% β-TCP/30% HA before grafting to ~62% β-TCP/38% HA after retrieval from the in vivo test.

As different scaffolds respond to in vivo tests in a different way also depending on their intrinsic morphometric characteristics, the retrieved specimens were analyzed in order to characterize their three-dimensional mineralized microarchitecture. These data are reported in Table 2 and clearly show that, neglecting some slight deviations (possibly due to the local differences in selected subvolumes), the biocoral scaffold offers performances comparable to the 70% β-TCP/30% HA one. Among the examined samples, the sample referred to the β-TCP block scaffold showed a mineralized volume (SV), a mineralized-to-TV, and a mean STh higher than all the other investigated samples. Consequently, also the specific surface of the mineralized structure (SS/SV) and the mean SNr were noticeably lower than in the other samples.

In Figure 4, a subvolume strictly referred to a portion of a β-TCP block is shown. In particular, in Figure 4B, the color map of the TCP wall thickness distribution is reported. The TCP block results in an assembling of single beads, each 350 to 400 μm thick, with some mismatches, fractures, and inhomogeneity possibly due to the harvesting process. Such inhomogeneity leads to a quite high mean strut spacing associated to a high mean STh (as observed in Table 2), which in turn results in an inhomogeneous distribution of microvessels (on the external grain borders, as observed in Figure 2B) and a small amount of regenerated bone (in correspondence of the location of the new vessels).

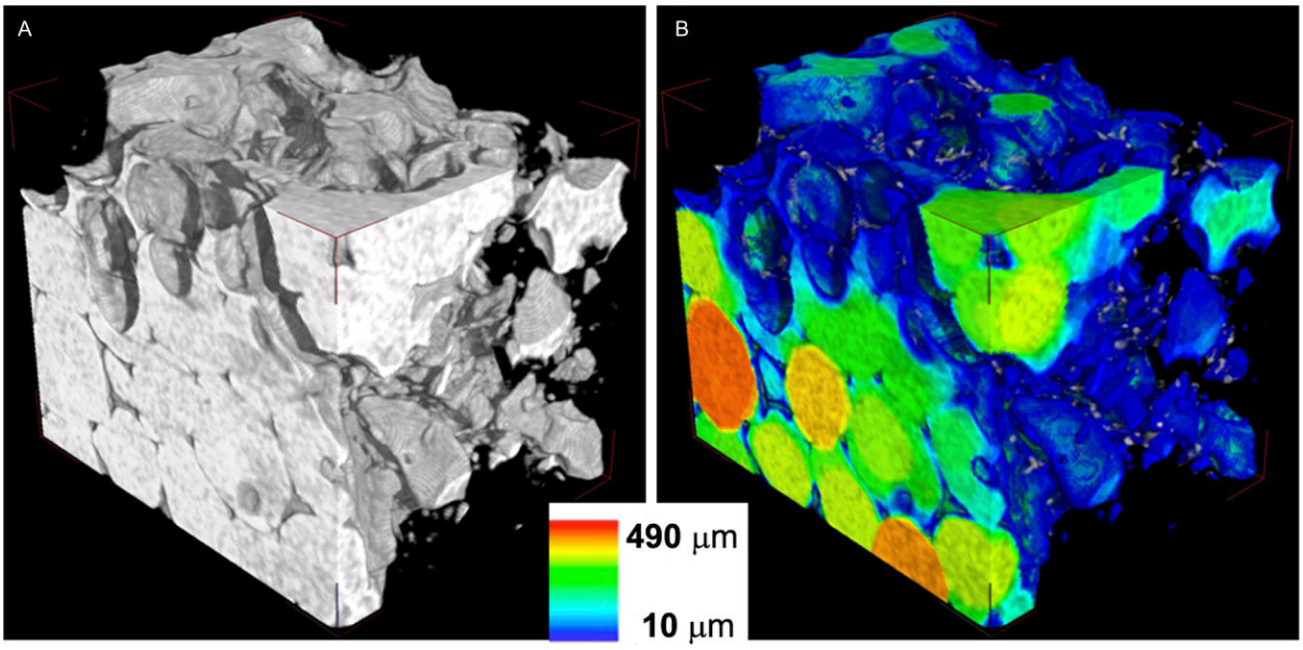

Figure 4 (A) Three-dimensional reconstruction of the sample made of Biocoral beads in combination with β-tricalcium phosphate (TCP) blocks: subvolume strictly referred to a portion of a β-TCP block. (B) Color maps of the wall thickness distribution in the same TCP block subvolume.

TABLE 6 Three-Dimensional Connectivity Analysis of the Constructs Retrieved from In Vivo Tests

	Pure Biocoral	Biocoral + TCP (volume I)	Biocoral + TCP (volume II)	70% TCP/30% HA
Connectivity index (mm^{-3})	6.4	10.9	2.8	22.9

HA = hydroxyapatite; TCP = tricalcium phosphate.

The structural analysis was repeated, this time only considering the regenerated bone phase: results are reported in Table 3. In this case, among the examined samples, the sample referred to Biocoral scaffolds showed bigger amount of newly formed bone (BV) combined with an increment of the BV-to-TV (BV/TV) ratio. Furthermore, they exhibited thicker mean trabecular thickness (TbTh) than the other investigated samples. Consequently, also the specific surface of the mineralized structure (BS/BV) was lower than in the other samples.

The TCP block sample showed also the worst morphometric characteristics in terms of newly formed bone with the lowest BV, BV-to-TV (BV/TV), and mean trabecular thickness (TbTh) with respect to all the other investigated specimens (Table 3). These morphometric data confirmed that, despite the optimal performances of the β-TCP material in bone TE,[43] the particular TCP block morphometric characteristics do not favor bone regeneration.

In agreement with the literature,[44] the TCP/HA scaffold exhibited good performances in terms of bone regeneration and vascularization, as reported in Table 3. In this case and differently from the Biocoral scaffold, the new bone regenerates in adhesion to the same scaffold that, on his turn, is only partially affected by resorption. In fact, with respect to the initial (pregrafting) volume percentages of the two scaffold phases, namely, 70 vol% TCP and 30 vol% HA, 6 to 7 months after grafting, the volume percentages were 62.5 vol% TCP and 37.5 vol.% HA, with the unique resorption of the TCP phase.

Tables 4 and 5 report the results of the anisotropy analysis of the samples (where isotropy index values close to 1 mean perfect isotropy and elongation index values close to 0 correspond to no preferred orientation). The sample referred to the β-TCP block is the most isotropic sample of the presented ones for both the scaffold and bone in-growth structure. Samples referred to Biocoral scaffolds are also rather isotropic for both the scaffold and bone structure. Sample 70% TCP/30% HA exhibits the least isotropic behavior of all the considered samples for both the scaffold and bone structure phase. Also, the elongation index for all the considered samples is rather close to zero, meaning that there are no preferred orientations in the $[u_1,u_2]$ plane.

In Table 6, the connectivity index is reported, which clearly shows that sample 70% TCP/30% HA has the most well-connected structures in between the scaffold-bone interface. The connectivity indexes of "pure Biocoral" and "Biocoral + TCP (volume I)" are rather close to each other, statistically confirming the stable behavior in vivo of the calcium carbonate material; meanwhile, the β-TCP-based block, namely, the "Biocoral + TCP (volume II)", has the most poorly connected structures of all the presented samples.

Histological Analysis

Histology evidences showed the presence of newly formed trabecular bone and residual grafted Biocoral biomaterial mainly located in the central area of the Biocoral specimen. The newly formed bone was in close contact with the biomaterial particles and, inside the biomaterial porous structure, it was possible to see some spaces colonized by newly formed bone, with areas of osteoid matrix undergoing mineralization (Figure 5, A and B).

Also, the retrieved TCP/HA-based sample presented portions characterized by newly formed bone trabeculae with small percentages of residual biomaterial and areas of tissue remodeling. The remaining biomaterial after the in vivo test was partially incorporated in the newly formed bone, while in other cases it was in the vicinity of the bone neoformation areas (Figure 5, C and D).

It has to be stressed that while BV/TV ratio, as extracted by micro-CT quantitative analysis and as shown in Table 3, is in the range of 29.0 to 30.5 vol% for the Biocoral-based samples and ~26.0 vol% for the TCP/HA-based one, histology showed that newly formed bone represented ~32.3 vol% for the Biocoral-based samples and ~37.3 vol% in retrieved TCP/HA-based samples.

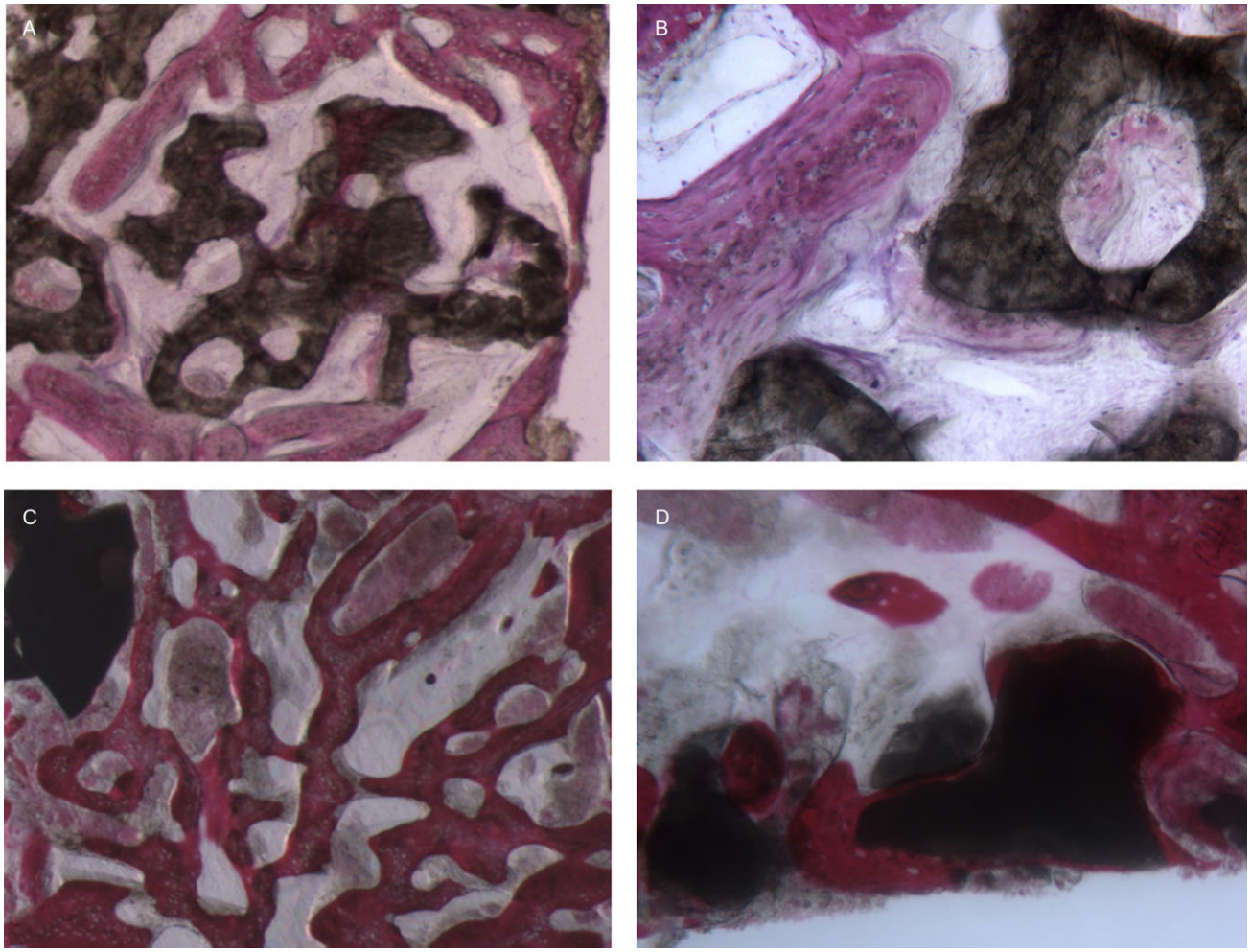

Figure 5 (A) Newly formed trabecular bone and residual grafted Biocoral particles (×40); (B) osteoid matrix, undergoing mineralization, inside the porous structure of the Biocoral biomaterial (×100); (C) newly formed trabecular bone and residual grafted hydroxyapatite (HA)/tricalcium phosphate (TCP) biomaterial (×40); and (D) newly formed bone around the TCP/HA structure (×100). Toluidine blue and acid fuchsin.

Due to the extremely poor and nonhomogeneous regenerative properties of the samples referred to the β-TCP block scaffolds, as documented in the literature and confirmed by micro-CT quantitative analysis, no histological analysis was performed on this sample.

DISCUSSION

In the present work, the three-dimensional porous architecture and microstructure of coralline-derived calcium phosphate scaffolds were investigated by synchrotron radiation x-ray microtomography after long-term in vivo tests on humans. The results were compared with those obtained on two different and selected samples, namely, a β-TCP block and a biphasic calcium phosphate porous scaffold both retrieved after in vivo test on humans for similar times. While the biphasic calcium phosphate was selected as control because of its good and documented in vivo performances as bone substitute, with several micro-CT studies reported in the last years literature,[20–22] the β-TCP block scaffold was tested in order to verify if, against the good bioactive properties of the biomaterial,[18,19] the unfavorable morphometric properties (reduced porosity and pore size) can play a critical role in the mechanism of its behavior as bone substitute.

Independently from the different volumetric dimensions of the retrieved Biocoral-based samples, it was observed that after the in vivo tests, a huge amount of bone is detected. This was demonstrated, after micro-CT histogram segmentation, by the wide peak area corresponding to the linear attenuation coefficient of the newly formed bone in Figure 2 and by

morphometric analysis reported in Tables 1 and 2. By micro-CT, it was also possible to detect a rich and well-distributed net of newly formed vessels in the retrieved Biocoral-based samples (evidences in Figure 3A). In fact, the selected synchrotron radiation experimental setup supplies also phase-contrast signal, allowing the visualization of these unmineralized tissues. It has to be stressed that information on the neovascularization is of paramount importance for the characterization of grafted scaffolds because vascularized areas constitute the sites where new bone formation is possible and favored.

Biocoral scaffold, as confirmed by histological results, was found to offer performances comparable or (considering specific aspects) better than the 70% β-TCP/30% HA control. In fact, the samples referred to Biocoral scaffolds showed bigger amount of newly formed bone (BV) combined to an increment of the BV-to-TV (BV/TV) ratio. Furthermore, they exhibited TbTh than the other investigated samples.

Samples referred to Biocoral scaffolds also appeared rather isotropic, both considering the whole mineralized structure (scaffold + newly formed bone – Table 4) and only bone structure (Table 5), with well-connected structures (Table 6).

In synthesis, the morphometric data, as extracted by micro-CT data analysis, demonstrate the good in vivo performances of the coralline-derived biomaterial (Biocoral) scaffolds for bone regeneration that, in turn, results homogeneously vascularized, resembling the natural cancellous bone, where trabeculae are irregular in shape and size. The good interconnectivity of scaffolds that open macropores is a valuable property expected to allow bone cell migration into the scaffold, bone in-growth, and implant vascularization in vivo.

By comparison of the Biocoral bioactivity with that referred to the three-dimensional scaffold composed by HA and β-TCP in the ratio of 30/70, it was observed that after the in vivo tests, a huge amount of bone is also detected, comparable to those referred to the Biocoral scaffolds. Furthermore, in analogy with the behavior of the Biocoral, an extended and uniform vascularization together with a huge amount of newly regenerated bone was observed (Figure 3C) in the 70% β-TCP/30% HA sample. In agreement with the literature,[45] we observed that, based on Table 1 quantitative analysis (but also as shown on the histogram reported in Figure 2C) for this specific sample, the TCP/HA scaffold exhibits good performances in terms of bone regeneration and vascularization. Bone regeneration is combined to the TCP resorption: in fact, the volumetric percentages modify from 70% β-TCP/30% HA before grafting to ~62% β-TCP/38% HA after retrieval from the in vivo test, with the unique resorption of the TCP phase. These data were confirmed by histology evidences.

Sample 70% TCP/30% HA experienced the least isotropic behavior of all the considered samples (Tables 4 and 5), but, even in this case, the elongation index is rather close to zero, meaning that there are no preferred orientations in the $[u_1,u_2]$ plane. This biphasic calcium phosphate-based sample was found to have the most well-connected structures (Table 6), indicating that the particular scaffold morphology may play a role in the hunt of the optimal scaffold structure to be implanted, regardless of the selected biomaterial.

The deviations between histology and micro-CT quantitative results in terms of volume percentages of regenerated bone demonstrate that the obtained three-dimensional micro-CT data represent very innovative progress as compared with the usual two-dimensional histological images, which do not provide the overall three-dimensional distribution of newly formed bone within the samples (with special reference to the TCP/HA-based one that seems highly inhomogeneous in terms of bone and biomaterial residue distribution).

However, the sample referred to the TCP block scaffold showed the worst morphometric characteristics in terms of newly formed bone: a small amount of regenerated bone, almost surrounding and in adhesion with the peripheral TCP grains, was detected with few vessels located as well in the peripheral regions of the TCP block. These data confirm that, despite the optimal performances of the β-TCP material in bone TE,[43] the particular TCP block morphometric characteristics do not favor bone regeneration. In fact, it is largely assessed that porosity and pore size of biomaterial scaffolds play a critical role in bone formation both in vitro and in vivo. According to the work of Hulbert and colleagues,[46] the recommended minimum pore size for bone TE scaffolds is 100 μm (subsequent studies have shown better osteogenesis for implants with pores above 300 μm[44,47,48]): in fact, large pores favor direct osteogenesis because they allow vascularization and high oxygenation.

In conclusion, this work confirms that micro-CT technique can play a fundamental role in advanced characterization of bone TE constructs because it allows,

in a noninvasive and nondestructive way, a complete, precise, and high-resolution three-dimensional analysis of their microstructural parameters.

ACKNOWLEDGMENTS

ELETTRA User Office is kindly acknowledged for providing beam time for the micro-CT experiments. The authors gratefully acknowledge the help of Sabine Hamisch, UweHamhaber, BioCerEntwicklungs-GmbH, Ludwig-Thoma-Str. 36c, 95447 Bayreuth, Germany, in providing the materials HA/β-TCP.

REFERENCES

1. Nerem RM. Cellular engineering. Ann Biomed Eng 1991; 19:529–545.
2. Langer R, Vacanti JP. Tissue engineering. Science 1993; 260:920–926.
3. Karageorgiou V, Kaplan D. Porosity of 3-D biomaterial scaffolds and osteogenesis. Biomaterials 2005; 26:5474–5491.
4. Hutmacher DW. Scaffolds in tissue engineering bone and cartilage. Biomaterials 2000; 21:2529–2543.
5. Middleton JC, Tipton AJ. Synthetic biodegradable polymers as orthopedic devices. Biomaterials 2000; 21:2335–2346.
6. Wang M. Developing bioactive composite materials for tissue replacement. Biomaterials 2003; 24:2133–2151.
7. Bostrom RD, Mikos AG. Tissue engineering of bone. In: Atala A, Mooney D, eds. Synthetic biodegradable polymer scaffolds. Basel: Birkhauser, 1997:215–234.
8. Hench LL. Bioactive materials: the potential for tissue regeneration. J Biomed Mater Res 1998; 41:511–518.
9. Ducheyne P, Qiu Q. Bioactive ceramics: the effect of surface reactivity on bone formation and bone cell function. Biomaterials 1999; 20:2287–2303.
10. Luginbuehl V, Meinel L, Merkle HP, Gander B. Localized delivery of growth factors for bone repair. Eur J Pharm Biopharm 2004; 58:197–208.
11. Ripamonti U. Osteoinduction in porous hydroxyapatite implanted in heterotopic sites of different animal models. Biomaterials 1996; 17:31–35.
12. Klein C, de Groot K, Chen W, Li Y, Zhang X. Osseous substance formation induced in porous calcium phosphate ceramics in soft tissues. Biomaterials 1994; 15:31–34.
13. Yuan H, Yang Z, de Bruijn JD, de Groot K, Zhang X. Material-dependent bone induction by calcium phosphate ceramics: a 2.5-year study in dog. Biomaterials 2001; 22: 2617–2623.
14. Mushipe MT, Revell PA, Shelton JC. Cancellous bone repair using bovine trabecular bone matrix particulates. Biomaterials 2002; 23:365–370.
15. Stock SR. X-ray microtomography of materials. Int Mater Rev 1999; 44:141–164.
16. Atwood RC, Jones JR, Lee PD, Hench LL. Analysis of pore interconnectivity in bioactive glass foams using X-ray microtomography. Scripta Mater 2004; 51:1029–1033.
17. Konerding MA. Scanning electron-microscopy of corrosion casting in medicine. Scanning Microsc 1991; 5:851–865.
18. Chappard D, Guillaume B, Mallet R, Pascaretti-Grizon F, Baslé MF, Libouban H. Sinus lift augmentation and beta-TCP: a microCT and histologic analysis on human bone biopsies. Micron 2010; 41:321–326.
19. Kim YH, Jyoti MA, Youn MH, et al. In vitro and in vivo evaluation of a macro porous β-TCP granule-shaped bone substitute fabricated by the fibrous monolithic process. Biomed Mater 2010; 5:1–11.
20. Komlev V, Mastrogiacomo M, Pereira RC, Peyrin F, Rustichelli F, Cancedda R. Biodegradation of porous calcium phosphate scaffolds in an ectopic bone formation model studied by x-ray computed microtomography. Eur Cell Mater 2010; 19:136–146.
21. Cancedda R, Cedola A, Giuliani A, et al. Bulk and interface investigations of scaffolds and tissue-engineered bones by x-ray microtomography and x-ray microdiffraction. Biomaterials 2007; 28:2505–2524.
22. Komlev VS, Mastrogiacomo M, Peyrin F, Cancedda R, Rustichelli F. X-ray synchrotron radiation pseudo-holotomography as a new imaging technique to investigate angio- and microvasculogenesis without use of any contrast agent. Tissue Eng Part C Methods 2009; 15:425–430.
23. Knackstedt MA, Arns CH, Senden TJ, Gross K. Structure and properties of clinical coralline implants measured via 3D imaging and analysis. Biomaterials 2006; 27:2776–2786.
24. Schliephake H, Zghoul N, Jager V, et al. Effect of seeding technique and scaffold material on bone formation in tissue-engineered constructs. J Biomed Mater Res 2009; 90A:429–437.
25. Kuboki Y, Takita H, Kobayashi D, et al. BMP-induced osteogenesis on the surface of hydroxyapatite with geometrically feasible and nonfeasible structures: topology of osteogenesis. J Biomed Mater Res 1998; 39:190–199.
26. Yukna RA. Clinical evaluation of coralline calcium carbonate as bone replacement graft material in human periodontal osseous defects. J Periodontol 1994; 65:177–185.
27. Pollick S, Shors EC, Holmes RE, et al. Bone formation and implant degradation of coralline porous ceramics placed in bone and ectopic sites. J Oral Maxillofac Surg 1995; 53: 915–922.
28. Roudier M, Bouchon C, Rouvillain JL, et al. The resorption of bone-implanted corals varies with porosity but also with the host reaction. J Biomed Mater Res 1995; 29:909–915.
29. Wikesjo UME, Lim WH, Razi SS, et al. Periodontal repair in dogs: a bioabsorbable calcium carbonate coral implant enhances space provision for alveolar bone regeneration in conjunction with guided tissue regeneration. J Periodontol 2003; 74:957–964.

30. Yukna RA, Yukna CN. A 5-year follow-up of 16 patients treated with coralline calcium carbonate (Biocoral) bone replacement grafts in intrabony defects. J Clin Periodontol 1998; 25:1036–1040.
31. Filmon R, Retailleau-Gaborit N, Brossard G, Grizon-Pascaretti F, Basle MF, Chappard D. Preparation of β-TCP granular material by polyurethane foam technology. Image Anal Stereol 2009; 28:103–112.
32. Deisinger U, Hamisch S, Schumacher M, Uhl F, Detsch R, Ziegler G. Fabrication of tailored hydroxyapatite scaffolds: comparison between a direct and an indirect rapid prototyping technique. Key Eng Mater 2008; 361–363:915–918.
33. Montanari F. SYRMEP TOMO PROJECT tutorial. Internet report, Sincrotrone Trieste; 2003.
34. Kak AC, Slaney M. Principles of computerized tomographic imaging. Society of Industrial and Applied Mathematics 2001. Originally published by IEEE Press at http://www.slaney.org/pct/pct-toc.html. (Accessed December 27, 2012).
35. Brun F, Mancini L, Kasae P, Favretto S, Dreossi D, Tromba G. Pore3D: a software library for quantitative analysis of porous media. Nucl Instrum Methods Phys Res A 2010; 615:326–332.
36. Parfitt AM. Bone histomorphometry: standardization of nomenclature, symbols, and units. Report of the ASBMR Histomorphometry Nomenclature Committee; 1987.
37. Whitehouse WJ. The quantitative morphology of anisotropic trabecular bone. J Microsc 1974; 101:153–168.
38. Harrigan TP, Mann RW. Characterization of microstructural anisotropy in orthotropic materials using a second rank tensor. J Mater Sci 1984; 19:761–767.
39. Cowin SC, Laborde AJ. The relationship between the elasticity tensor and the fabric tensor. Mech Mater 1985; 4:137–147.
40. Cowin SC. Wolff's law of trabecular architecture at remodeling equilibrium. J Biomech Eng 1986; 108:83–88.
41. Odgaard A, Gundersen HJ. Quantification of connectivity in cancellous bone, with special emphasis on 3-D reconstructions. Bone 1993; 14:173–182.
42. Benn DI. Fabric shape and the interpolation of sedimentary fabric data. J Sediment Res 1994; 64:910–915.
43. Kato E, Lemler J, Sakurai K, Yamada M. Biodegradation property of beta-tricalcium phosphate-collagen composite in accordance with bone formation: a comparative study with Bio-Oss Collagen® in a rat critical-size defect model. Clin Implant Dent Relat Res 2012. DOI: 10.1111/j.1708-8208.2012.00467.x.
44. Gotz HE, Muller M, Emmel A, Holzwarth U, Erben RG, Stangl R. Effect of surface finish on the osseointegration of laser-treated titanium alloy implants. Biomaterials 2004; 25:4057–4064.
45. Piattelli A, Scarano A, Mangano C. Clinical and histologic aspects of biphasic calcium phosphate ceramic (BCP) used in connection with implant placement. Biomaterials 1996; 17:1767–1770.
46. Hulbert SF, Young FA, Mathews RS, Klawitter JJ, Talbert CD, Stelling FH. Potential of ceramic materials as permanently implantable skeletal prostheses. J Biomed Mater Res 1970; 4:433–456.
47. Kuboki Y, Jin Q, Takita H. Geometry of carriers controlling phenotypic expression in BMP-induced osteogenesis and chondrogenesis. J Bone Joint Surg Am 2001; 83A:S105–S115.
48. Tsuruga E, Takita H, Itoh H, Wakisaka Y, Kuboki Y. Pore size of porous hydroxyapatite as the cell-substratum controls BMP-induced osteogenesis. J Biochem 1997; 121: 317–324.